Optical Materials 64 (2017) 524–532

Contents lists available at ScienceDirect

Optical Materials

journal homepage: www.elsevier.com/locate/optmat

UV-transmitting step-index fluorophosphate glass fiber fabricated by the crucible technique

Gustavo Galleani [a, b, *], Yannick Ledemi [b], Elton Soares de Lima Filho [b], Steeve Morency [b], Gaëlle Delaizir [c], Sébastien Chenu [c], Jean René Duclere [c], Younes Messaddeq [b]

[a] Institute of Chemistry, São Paulo State University/UNESP, Araraquara, SP, Brazil
[b] Center for Optics, Photonics and Lasers, Laval University, Québec, QC, Canada
[c] Laboratoire de Sciences des Procédés Céramiques et de Traitements de Surface, Université de Limoges, Limoges, France

ARTICLE INFO

Article history:
Received 24 October 2016
Received in revised form
28 December 2016
Accepted 4 January 2017
Available online 17 January 2017

Keywords:
Glass
Fibers
Fluorophosphate
Crucible method
UV transmitting materials

ABSTRACT

In this study, we report on the fabrication process of highly pure step-index fluorophosphate glass optical fibers by a modified crucible technique. High-purity fluorophosphate glasses based on 10 mol% of barium metaphosphate and 90 mol% of metal fluorides (AlF_3–CaF_2–MgF_2–SrF_2) have been studied in order to produce step-index optical fibers transmitting in the deep-ultraviolet (DUV) region. The characteristic temperatures, viscosity around softening temperature and optical transmission in the UV–visible region of the prepared bulk glasses were characterized in a first step. The selected glass compositions were then used to prepare core-cladding optical preforms by using a modified built-in casting technique. While uncontrolled crystallization of the fiber was observed during the preform stretching by using the conventional method, we successfully obtained crystal-free fiber by using a modified crucible technique. In this alternative approach, the produced core-cladding preforms were inserted into a home-designed fused silica crucible assembly and heated at 643 °C to allow glass flowing throughout the crucible, preventing the formation of crystals. Single index fluorophosphate glass fibers were fabricated following the same process as well. The optical attenuation at 244 nm and in the interval 350–1750 nm was measured on both single index and step-index optical fibers. Their potential for using in DUV applications is discussed.

1. Introduction

The development of new optical fibers capable of operating in the ultraviolet (UV) region would benefit the fast remote elemental analysis of non-metallic elements of first environmental or industrial importance. For instance, elemental phosphorus exhibits its principal emission lines in the vacuum-UV region (VUV, <200 nm) at 177.50, 178.29 and 178.77 nm, or a less sensitive one in the deep-UV region (DUV, <300 nm) at 213.62 nm [1]. Laser-induced breakdown spectroscopy (LIBS) has been applied for elemental detection for solid, liquid or gas samples [2], where powerful laser pulses are used to form a microplasma or a spark on the sample to analyze. An optical fiber can be then employed to remotely collect and transmit the plasma/spark light from relatively long distances to the detection system to quantify the emitting species [3–5]. The well-established commercial UV-transmitting optical fibers are based on high–OH–silica glass. However, the latter is usually rapidly damaged under UV light exposure owing to absorption by pre-existing or radiation induced defects, causing an abrupt increase of the absorption losses below 250 nm [6–8]. This restricts thus their use for a short-period and a periodic replacement is required for these fibers. As long-term stability of light transmission is highly desirable in optical system design, the development of alternative UV-transmitting optical fibers is of major importance.

Glasses based on beryllium fluoride or aluminum and alkaline earth metal fluorides with wide band gap exhibit an extended optical transmission in the UV down to 160 nm [9,10]. However, on one hand beryllium fluoride is extremely toxic and its use is discouraged. On the other hand, fluoroaluminate glasses are known for their tendency to crystallize upon heating up to drawing temperature due to reaction of the glass with moisture in the

* Corresponding author. Institute of Chemistry, São Paulo State University/UNESP, Araraquara, SP, Brazil.
E-mail address: gugalleani@yahoo.com.br (G. Galleani).

http://dx.doi.org/10.1016/j.optmat.2017.01.017
0925-3467/

processing environmental atmosphere, limiting the fabrication of vitreous fiber [11]. Since these disadvantages result primarily from the strong ionic character of fluoride glasses, considerable progress in the glass forming ability can be made by the addition of small amount of phosphate. Fluorophosphate glasses produced by mixing fluorides (mainly, AlF_3 and MF_2, M = Sr, Ca, Mg, Ba) and phosphates ($Sr(PO_3)_2$, $Ba(PO_3)_2$, $Al(PO_3)_3$ and $NaPO_3$), were extensively studied [12–16]. These mixed glasses have shown a combination of many desirable properties from the phosphate and fluorides components, including excellent glass-forming abilities, low refractive indices, low partial dispersion, and broad transmission window ranging from ~160 nm to 4000 nm. Optical transmission in the deep-UV is only achieved when the glasses are prepared from ultra-high-purity starting materials, since the main limitation is the extrinsic absorption by transition metal impurities in the ppm range [13–15]. Unlike silica glass, fluorophosphate glasses with low phosphate content and ultra-high chemical purity may exhibit low loss transmission in the UV region owing to the absence of absorption/scattering defect centers [17,18]. Achieving ultra-low losses in fluorophosphate glass fibers similar to those attained in silica fibers (whose technology is mature nowadays), might open new possibilities for UV-transmitting optical fibers for the above mentioned applications. For a better understanding, it is worth distinguishing here the terms highly pure and low loss from ultra-highly pure and ultra-low loss, respectively. The former stands for optical materials prepared from starting materials of 5N chemical purity or higher (i.e. with impurity levels in the ppm range) while the latter stands for materials of higher purity (i.e. with impurity levels in the ppb range). Moreover, ultra-highly pure fluorophosphate glasses may also show a better long-term radiation resistance to UV light [19] since their optical basicity (electron donor power of the glass matrix) is lower in comparison with silica glass, due to a lower content of non-bridging oxygens when the phosphate content is low. The UV radiation damage of such glass is known to be directly related to the amount of phosphate groups and the presence of metallic impurities within the glassy network [15,16,18–21].

Very few studies on the fabrication of fluorophosphate glass optical fibers have been reported in the literature [17,18,22,23]. Zou et al. produced step-index fibers by drawing at the optical tower an ultra-highly pure core-cladding preform obtained by extrusion in the system P_2O_5–AlF_3–YF_3–MgF_2–RF_2–NaF, (R = Mg, Ca, Sr and Ba). The minimum loss they measured in the UV was 0.11 dB/m at 365 nm [17]. Kalnins et al. have prepared an unclad optical fiber by drawing preforms produced by extrusion under nitrogen of a commercial fluorophosphate glass (N-FK51A). Although they reported on preform neck-down crystallization issues during the drawing, they achieved minimum losses of 3.05 dB/m at 405 nm after increasing the preform feed-rate and drawing speed [22]. They also showed that treatment of extruded preforms prior to fiber drawing further improved optical fiber loss to 0.5–1 dB/m [23].

In this paper, we report on the fabrication of high-purity fluorophosphate glass optical fibers transmitting in the UV. We optimized the fluoride/phosphate ratio content to achieve a highly transparent glass in the DUV region with a large thermal stability against crystallization for further fiber drawing. Core-cladding preforms were first prepared by a modified build-in casting method [24,25]. As we faced surface crystallization issues during fiber drawing from the preforms, an alternative fiber fabrication process was then implemented. This approach, derived from the well-known double crucible method [26–32], consisted in drawing the core-cladding fibers from the as-prepared preforms throughout a simple crucible. Finally, the optical transmission losses in the UV and IR regions of the successfully produced fibers were measured and the potential of this new fiber fabrication process was discussed.

2. Experimental procedure

2.1. Bulk glass synthesis

Fluorophosphate glass samples of compositions $10Sr(PO_3)_2$-$90(AlF_3$–CaF_2–MgF_2–$SrF_2)$ and $xBa(PO_3)_2$-100-$x(AlF_3$–CaF_2–MgF_2–$SrF_2)$, with x = 5, 10 and 20 mol% were prepared by the conventional melt-quenching method from mixed high-purity fluorides, AlF_3 (MV labs, 99.999%), SrF_2 (Sigma, 99.995%), CaF_2 (Sigma 99.99%), MgF_2 (Cerac, 99.999%) and metaphosphate $M(PO_3)_2$ (M = Ba and Sr). High-purity barium and strontium phosphates were prepared from the solid state reaction of $NH_4H_2PO_4$ (Sigma, 99.999%) with MCO_3 (Alfa Aesar, 99.994%):

$$MCO_3(s) + 2(NH_4)H_2PO_4(s) \rightarrow M(PO_3)_2(s) + CO_2(g) + 3H_2O(g) + 2NH_3(g).$$

The mixed powders were loaded in a platinum crucible, heated at 250 °C at a rate of 5 °C.min^{-1} and kept at this temperature during 24 h to allow a complete reaction of the precursors. The mixture was subsequently heated at 500 °C in an electric furnace for 1 h to eliminate the gas in excess formed during the reaction. After the reaction, the appropriate amount of the corresponding metaphosphate was mixed with the fluorides starting materials, loaded into a capped carbon crucible and melted at 1000 °C in an induction furnace. The resulting liquid was kept at this temperature for 30 min to ensure fine homogenization. Finally, the melted glasses were cooled rapidly in a brass mold at the glass transition temperature. The glass was then placed into a resistive oven at the annealing temperature for 4 h and subsequently cooled down to room temperature in approximately 10 h to remove any residual stress induced during the quenching. The glass samples were polished using silicon carbide polishing paper with decreasing grit size (400, 600, 800, 1200) before using a 1 μm diamond suspension to obtain a good surface quality for optical characterization.

2.2. Core-cladding preform preparation and optical fiber drawing

As mentioned in the introduction, an alternative method was implemented to produce the step-index fluorophosphate glass fibers. This method, which will be discussed in more details later, consists in two successive steps: (i) the fabrication of core-cladding preforms by the conventional build-in casting method [24,25] and; (ii) the drawing of the step-index fibers from the as-prepared preforms through a fused silica crucible. First, to prepare the core-cladding preforms, cylindrical glass tubes with the cladding composition $[10Sr(PO_3)_2$-$90(AlF_3$–CaF_2–SrF_2–$MgF_2)]$ were first prepared. Then, cylindrical glass rods with the core composition $[10Ba(PO_3)_2$-$90(AlF_3$–CaF_2–SrF_2–$MgF_2)]$ were prepared separately, either following in a two-step discontinuous melting system. For both glass tubes and rods, the raw materials were first pre-melted at 1000 °C for 30 min, like for the bulk glass synthesis (see Section 2.1). Then, the glasses were re-melted under vacuum at 730 °C for 1 h and poured into a cylindrical brass mold preheated at the glass transition temperature and annealed at the same temperature for 6 h. To produce the glass rods for the preform core, a cylindrical mold of 5 mm inner diameter was employed. To produce the glass tube for the preform cladding, a modified built-in casting technique was used [24]: (i) the glass is cast into the preheated mold of 10 mm inner diameter and begins to solidify in contact with the mold walls; (ii) a shutter placed below the mold is then opened, allowing the part of the glass which is still liquid (center of the cylinder) to flow away, forming a glass tube and; (iii) the same shutter is closed

once the tube has solidified with the desired diameter and length.

Second, to produce the fibers, the glass rod was manually inserted into the glass tube and the as-assembled core-cladding preform was then loaded into the fused silica crucible, as illustrated in Fig. 1. The assembly was then placed into the drawing furnace while argon gas was flowing around the crucible. The temperature of the furnace was raised to 672 °C (Tg + 222 °C) for a period of 20 min to allow the glass to flow to the crucible nozzle (out of the heating zone of the furnace). The furnace temperature was then lowered to 643 °C (Tg + 193 °C) and the fiber drawing process was started. It is worth mentioning that the temperature values given here are those read by the temperature controller in the furnace. The actual temperature of the glass within the crucible may be slightly different. During the process, a low-index UV-cured polymer coating (DeSolite® DF-0007) was applied to the fiber surface to improve its mechanical resistance.

A single-index fiber coated with the low-index UV-cured polymer jacketing was also produced by the same method, drawing a rod with the core composition.

2.3. Material characterization

2.3.1. Thermal characterization

Differential scanning calorimetric (DSC) measurements were performed using a Netzsch DSC Pegasus 404F3 apparatus on 25 mg glass pieces into Pt pans at a heating rate of 10 °C min^{-1} up to a temperature of 750 °C under nitrogen atmosphere.

Temperature dependence of viscosity in the range 10^7-10^{11} Poise was measured with a Bansbach Easylift Theta US parallel plate high temperature viscometer. Cylindrical samples were slices cut from annealed glass rods with 10 mm diameter and 6 mm thickness and sandwiched between two silica plates inside a well-insulated furnace under nitrogen flow and heated at a heating rate of 2 °C/min, under a compressive load of 300 g. By means of recording the rate of the thickness change of the sample as a function of time (using a linearly variable differential transformer (LVDT)), the logarithm of viscosity *vs* temperature is determined by the Dilasoft program. The estimated error was about ±3 °C on the temperature values and ~$10^{\pm 0.2}$ Poise on the viscosity values.

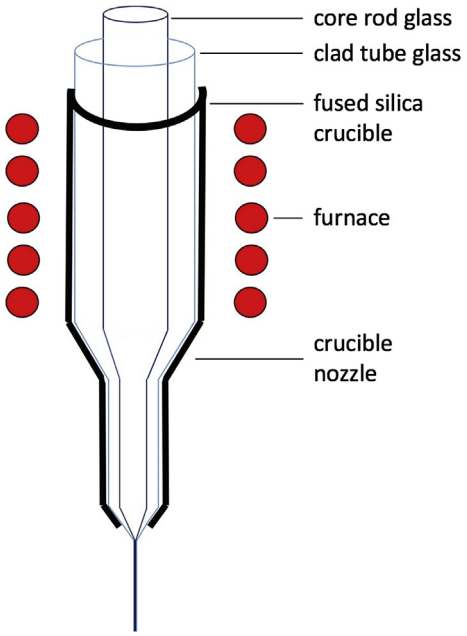

Fig. 1. Fused silica crucible assembly used for fiber drawing.

2.3.2. Optical characterization

Glass sample transmission spectra have been measured by using a UV-VIS-NIR Varian Cary 5000 double beam spectrophotometer from 185 to 800 nm on polished samples. Since oxygen from ambient atmosphere absorbs in the range 185–200 nm, an adapted nitrogen purge was used in the sample chamber for the measurements.

Linear refractive index n has been extracted from ellipsometry measurements, using a Horiba Jobin-Yvon UVISEL Extended Range spectroscopic ellipsometer, operated in the 200–800 nm wavelength range. The angle of incidence was fixed at 60° and the light spot size was 1 mm in diameter.

The fiber transmission losses were measured at the wavelength $\lambda_1 = 244$ nm and in the range 350 nm $\leq \lambda_2 \leq$ 1750 nm. For the measurement at λ_1, a Coherent Innova 300c laser was used as optical source. The laser beam was chopped at 1 kHz using a Thorlabs MC2000 optical chopper. The input and output of the fiber were manually cleaved. A CaF_2 lens of 40 mm focal length was used to inject light into the fiber, which was placed in a clamp in a three-axis fiber coupling stage. The distal end of the fiber was clamped into a SMA adaptor, which was used both for fiber alignment, as well as to block stray light. The fiber output power was detected using a Si photodiode S120VC from Thorlabs, interrogated by a Thorlabs PM100D power meter and a Lock-in amplifier SR830 DSP, from Stanford Research. For the broadband measurement, the input of the optical fiber was clamped at the focus of an in-house built tungsten-halogen lamp housing, and the output connected directly to an optical spectrum analyzer (OSA), Yokogawa AQ-6315A. In both measurements, the fiber was cut in several sections, and the output power was measured for each section. This allows obtaining accurate transmission losses through a multiple-point cut-back method.

3. Results and discussion

3.1. Bulk glasses characterization

In mixed fluorophosphate glass systems, it is known that an increase of the phosphate content results in decreasing the optical transmission in the UV region, since the phosphate content decreases the band gap energy [14]. Therefore, to produce a fiber transmitting deeper in the UV, one has to consider a glass with good thermal stability with a phosphate content as low as possible. For this reason, three fluorophosphate glass samples containing 5, 10 and 20 mol% of phosphate were prepared and characterized to select the most appropriate composition for further fiber drawing tests.

Fig. 2 shows the DSC curves obtained for the glasses $xBa(PO_3)_2$-100-x (AlF_3–CaF_2–SrF_2–MgF_2) with x = 5, 10 and 20 mol%, labelled as 5BaPF95, 10BaPF90 and 20BaPF80, respectively. An important factor to consider prior to any fiber drawing is the thermal stability against crystallization $\Delta T = Tx - Tg$, where Tg is the glass transition temperature determined from the endothermic baseline shift of the DSC curve while Tx is the onset temperature for the first crystallization exothermic peak. The larger is ΔT, the lower is the risk of observing formation of crystals while drawing the fiber, taking into account that the drawing temperature (643 °C here), which depends on the viscosity vs temperature behavior, is relatively far from the crystallization temperature Tx (748 °C here). The Tg increases from 439 °C to 460 °C with increasing phosphate content while the crystallization peak broadens, which can be related to an increase of the glass forming ability due to the insertion of more covalently bonded PO_4 groups in the fluoroaluminate structure. In

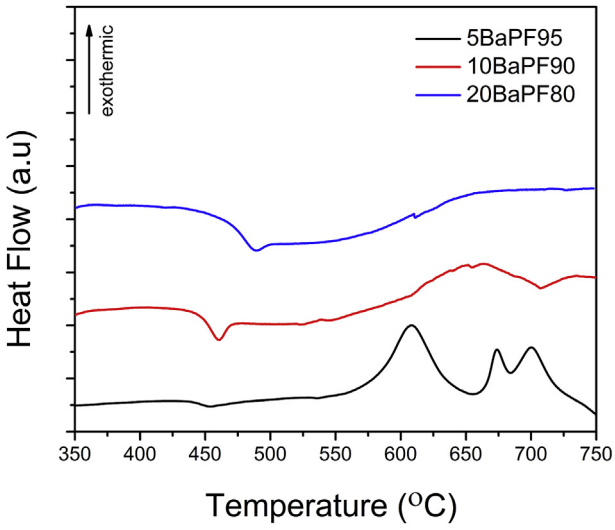

Fig. 2. DSC curves of the studied fluorophosphate glasses $xBa(PO_3)_2$-90-x(AlF_3, CaF_2, MgF_2, SrF_2), x = 5, 10 and 20 mol%, respectively labelled as 5BaPF95, 10BaPF90 and 20BaPF80.

the fluoroaluminate glasses, AlF_6-octahedra connected by shared corners are proposed as the main glass forming entity [33]. In the fluorophosphate glasses, the structure consists of interconnected $Al(O/F)_6$—octahedra and PO_4-tetrahedra cross-linked by modifier cations, which increases the rigidity of the structure, limiting and slowing the nucleation process [34,35]. For the 5BaPF95 and 10BaPF90 samples, the thermal stability are 95 °C and 149 °C, respectively, and for the 20BaPF80 sample, the onset of crystallization is difficult to be precisely determined, as can be seen in Fig. 2. The glass 10BaPF90, with higher thermal stability compared with 5BaPF95, has been chosen for the core-cladding step-index fiber fabrication, and $Ba(PO_3)_2$ was replaced by $Sr(PO_3)_2$ in the cladding glass composition (labelled 10SrPF90) to decrease its refractive index in view of preparing a step-index glass preform.

The transmission spectra from the DUV-visible to the infrared region of the glass samples selected for the fabrication of the core-cladding step-index fiber are shown in Fig. 3a and b, respectively. In the literature, an intrinsic VUV edge of fluorophosphate glasses containing 10 mol% of phosphate was reported at 160 nm [36]. The same authors also pointed out the strong influence of extrinsic absorptions from transition metal impurities present in the glasses on their VUV cut-off edge. In the present work, the transmission in the UV region reaches 90% above 240 nm and is nearly 75% at 180 nm (below this wavelength, a special equipment for the vacuum ultraviolet region is needed). At 220 nm, a small absorption peak is observed, which is due to Fe^{2+} impurity absorption. Iron is the main trace impurity of fluoride and phosphate raw materials. Erht et al. have shown that glasses melted under reducing conditions possess better transmittance in the UV, since the redox state of iron traces, Fe^{3+} (absorption band at 250 nm and 185 nm), can be almost completely shifted to Fe^{2+} (absorption band at 220 nm and 170 nm) with lower molar absorption coefficient $\varepsilon_{i\lambda}$ (cm^{-1}.ppm^{-1}) [37]. Even small amounts of iron impurities (ppm range) can cause high optical losses in the final glass and fiber. To our knowledge, the transmission spectra presented here are comparable to the best results reported in the literature on fluorophosphate bulk glasses of 2 mm thickness [36]. In the latter work, glasses showing about 80% of transmission at 200 nm were produced from high purity starting materials and the final iron content in the glass was measured to be 6 ppm.

The absorption coefficient α_{220nm} at 220 nm was determined

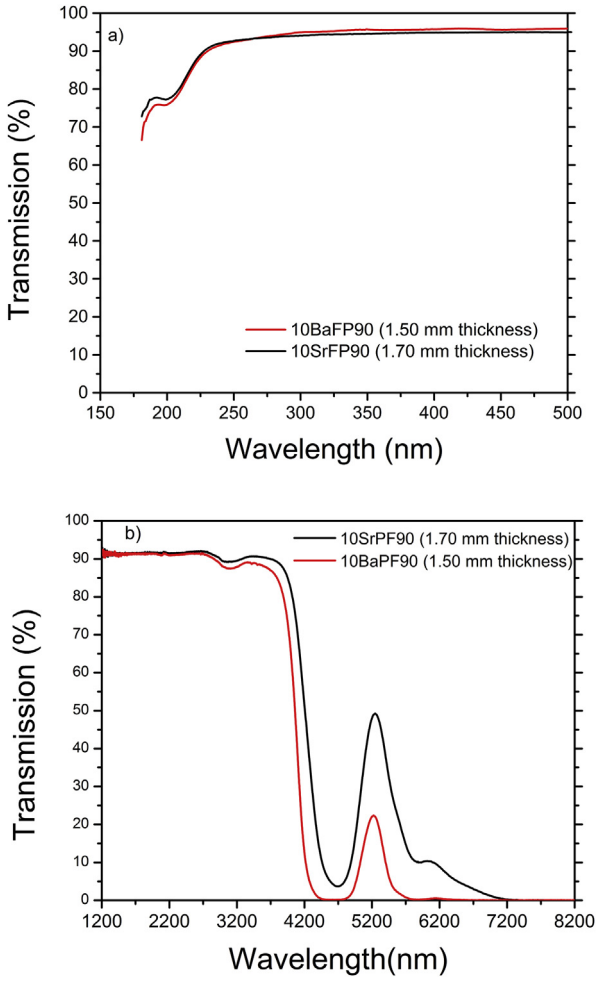

Fig. 3. (a) Deep-UV and (b) infrared transmission spectra, for the core and cladding glasses with 1.50 and 1.70 mm thickness, respectively.

from the transmission spectrum. By using the Beer-Lambert law.

$$\alpha = \ln\left(\frac{T_0}{T}\right)\Big/ l \tag{1}$$

where l, T_0 and T represent the sample thickness, the maximum transmittance (%) of the glass matrix and the transmittance at 220 nm, respectively. For the cladding glass (10SrPF90), $\alpha_{220} = 1.25\ cm^{-1}$ and for the core glass (10BaPF90), $\alpha_{220} = 1.54\ cm^{-1}$.

In the IR region, the transmission reaches 91% and extends up to 4000 nm. The absorption peak around 3000 nm is ascribed to O—H stretching. The infrared edge at 4500 nm is due to the P—O vibration [38].

The evolution of the refractive index measured on the core and cladding glasses as a function of wavelength is shown in Fig. 4. Measuring the refractive index in the UV region is a complex task. Here, ellipsometry that reflects polarized light from bulk sample and detects the change in polarization introduced by the sample structure was used to reconstruct the index profile. The curve for the core and cladding glass was fitted by using the Cauchy dispersion formula:

$$n(\lambda) = A + \frac{B}{\lambda^2} + \frac{C}{\lambda^4}$$

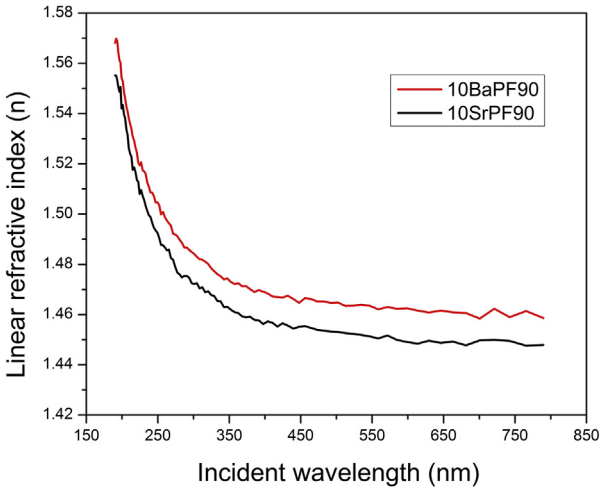

Fig. 4. Dispersion curves for the core (10BaPF90, red line) and cladding (10SrPF90, black line) glass compositions, determined from ellipsometry measurements. (For interpretation of the references to colour in this figure legend, the reader is referred to the web version of this article.)

The coefficients associated with the curve are A = 1.45599, B = 7.457 × 10^{-16} m^2 and C = 1.2874 × 10^{-28} m^4 and A = 1.44794, B = 7.2197 × 10^{-16} m^2 and C = 1.12542 × 10^{-28} m^4 for the core (10BaPF90) and cladding (10SrPF90) glass, respectively. It is worth noting that the Cauchy formula was preferred here to the Sellmeier formula which is generally used to fit the refractive index wavelength dispersion in a broader range. However, here, we measured the dispersion only in the UV–visible range of interest, and the Cauchy dispersion proved to display a better fitting than the Sellmeier dispersion, compared to the experimental data. The index difference between the core and cladding glasses is 0.013 at 244 nm, which corresponds to a numerical aperture of 0.19. Thermal and optical properties of the glasses are summarized in Table 1.

3.2. Core-cladding glass preform fabrication and fiber drawing

The two principal methods known to fabricate optical fibers are the solid glass preform drawing and the double crucible technique. The first technique requires to prepare a solid glass preform of desired dimensions, geometry, structure, etc. that will be further stretched at the optical fiber drawing tower at a temperature corresponding to a specific viscosity, as discussed later. Such technique is widely employed to draw vitreous materials which are highly stable against crystallization *vs* temperature. Nevertheless, surface crystallization or formation of bubbles issues while drawing the preform into fiber can eventually occur even with highly stable glassy materials, such as the fluorophosphate glasses under study here. In the second method, the double crucible technique, core and cladding glasses are prepared separately to feed each crucible, one for the core and the other for the cladding, where they are heated at a larger temperature than in the previous method to enable the flowing of both core and cladding glasses through the crucible. Such approach not only permits to limit the surface crystallization issues, but it may also improve the quality of core/cladding interface. This method, well-known in the field of optical fiber fabrication but rarely employed because of its complex implementation, was first designed for fluoride glasses more than 30 years ago [27]. It was also employed to produce oxyfluoride fibers [28] and more largely for the fabrication of step-index chalcogenide soft glasses for infrared applications [29–32]. Nevertheless, such method is rather more complex to implement from a practical point of view than the first one.

To prepare solid glass preforms, a core-cladding preform in our case, the main techniques are the extrusion technique [17,39] and the rod-in-tube technique which implies the use of the rotational or the build-in casting techniques to form the cladding glass tube [24,25]. In this work, a modified build-in casting technique similar to that reported in Ref. [24] was used. Prior to the core-cladding preform fabrication, a re-melt of the glasses under vacuum step was applied, as described in section 2.2. Indeed, a release of gas followed by the formation of bubbles (probably coming from dissolved gas in the glass melt) was observed in the first attempts to draw the fibers from the preforms, causing many imperfections in the fibers. The re-melt step has permitted to decrease the amount of gas dissolved in the melt that seems to be less soluble at lower temperature (700 °C in the re-melt step) than at higher temperatures (1000 °C in the first melt step), improving the fiber quality. Perhaps HF gas is released at higher temperature and trapped after glass formation.

The cladding tube and the core rod glass preform used for drawing are shown in Fig. 5. The length of the preforms was about 11 cm. For the tube, the external and internal diameters are 10 and 5 mm, respectively (Fig. 5a), for the rod the diameter was 4 mm (Fig. 5b).

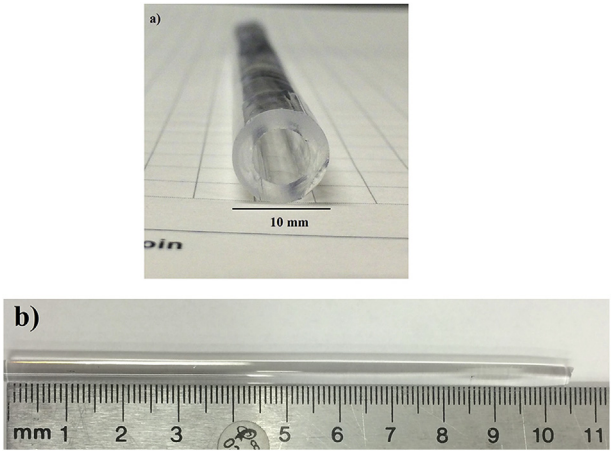

Fig. 5. Photographs of the cladding glass tube (a) and the core glass rod (b).

Table 1
Main characteristics of the glasses under study, including glass transition temperature Tg, onset temperature of crystallization Tx, thermal stability against crystallization ΔT = Tx − Tg and linear refractive index n at 250 nm (determined from ellipsometric measurement).

Glass label	Composition (mol%)						Tg (±2 °C)	Tx (±2 °C)	ΔT = Tx − Tg (±4 °C)	n at 250 nm
	$Ba(PO_3)_2$	$Sr(PO_3)_2$	AlF_3	CaF_2	MgF_2	SrF_2				
5BaPF95	5	–	38	25	11	21	439	534	95	–
10BaPF90	10	–	35	30	10	15	450	599	149	1.505
20BaPF80	20	–	32	21	9	18	460	–	–	–
10SrPF90	–	10	35	30	10	15	447	597	150	1.492

The DSC curve and the viscosity data near glass softening point recorded on the core glass (10BaPF90) and cladding glass (10SrPF90) are shown in Fig. 6. The co-drawing of two glass materials of different compositions usually requires an excellent matching of their thermal properties, including viscosity vs. temperature. Key parameters as thermal stability against crystallization and viscosity (η) vs temperature (T) are used to evaluate the glass forming ability and the range of temperature for fiber drawing [40]. The glass transition temperatures Tg measured on the 10SrPF90 glass tube and the 10BaPF90 glass rod are 447 °C and 450 °C, respectively while their thermal stability against crystallization are 150 °C and 149 °C, respectively. Such thermal stability is well above the 100 °C usually considered as a minimum value to allow glass stretching without crystallization.

The evolution of log (η) vs T (Poise/°C) near the glass softening region is approximately linear, as the Arrhenius approximation applies and decreases rapidly with increasing temperature. Depending on the method used to draw optical fibers, i.e. preform drawing or crucible technique, the required glass viscosity is not the same. In the crucible technique, a low viscosity varying around 10^2-10^3 Poise is needed as the glass has to flow through the crucible whereas a slightly larger viscosity ranging between $10^{5.5}$-10^6 Poise enables the fiber drawing from the glass preform. After extrapolating the viscosity curves recorded as a function of temperature, we can obtain the intercepts of the temperatures accordingly with the required viscosities corresponding to each method, as depicted in Fig. 6. Fiber fabrication from preform drawing is therefore expected to be achieved around 540–560 °C whereas a temperature of about 600–620 °C will be necessary to produce fiber through the crucible technique. As can be seen in Fig. 6, these estimated temperatures for fiber drawing are very close to the onset of crystallization as determined for the core and cladding glasses by DSC, 597 °C and 599 °C, respectively. It is worth reminding that the heating rates used for each characterization technique were different (10 °C/min for the DSC and 2 °C/min for viscosity measurements). Nevertheless, a large change of viscosity with respect to a small variation of temperature is clearly observed here. Minimizing the time spent by the preform at the drawing temperature was therefore considered as a crucial requirement to avoid crystallization during the fabrication process, as well as using a fast drawing rate and a small hot zone in the drawing furnace.

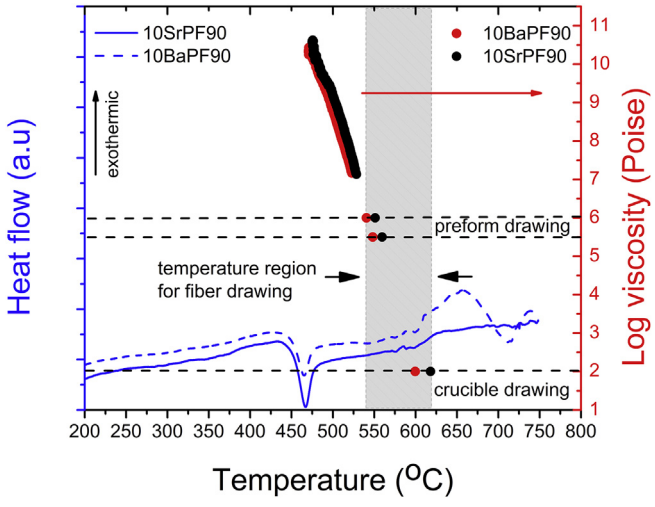

Fig. 6. DSC curves and viscosity recorded by the parallel plate method as a function of temperature of the core (10SrPF90, black line) and cladding (10BaPF90, red line) glass compositions. The heating rate was 10 °C/min for the thermal analysis and 2 °C/min for the viscosity measurement. (For interpretation of the references to colour in this figure legend, the reader is referred to the web version of this article.)

From an experimental point of view, the first avenue explored to produce the fluorophosphate fibers was by simply drawing core-cladding optical preforms. However, despite the fact that this method seemed to be successful in the work of Zou et al. [17,18], we were not able to draw a crystal-free optical fiber from neither a core-cladding preform nor a single index preform. On the contrary, we rapidly faced serious problems of uncontrolled crystallization at the surface of the fiber during the fiber drawing process, similar to those reported by Kalnins et al. [22]. Surface crystallization issues were also reported in fluoroaluminate glass fiber drawing and ascribed to moisture attack followed by surface devitrification along the drawing process [41]. It is worth mentioning that the purity of the starting materials used in the work of Zou was similar to that of our used precursors (4N or above). We can thus assume that the precursors' purity is not playing a role in the crystallization issues observed during the preform drawing. Our first attempts were conducted under dry nitrogen atmosphere around 545 °C and it was not possible to draw fiber pieces longer than around 2 m because of the formation of crystals which dramatically degrade the fiber strength.

After numerous unfruitful trials varying the process parameters (temperature, preform feeding speed, time spent in the drawing furnace, nature and pressure of gas, etc.) where crystallization traces were always observed in the preform neck-down and the drawn fibers, the use of an alternative approach was found to be more successful. This alternative method consisted in drawing the core-cladding preform through a home-made fused silica crucible. To some extent, this method combines both the techniques above described. The core-cladding preform was thus inserted in a cylindrical fused silica crucible and heated at 643 °C, which is slightly above the temperature corresponding to the 10^3–10^2 Poise viscosity required for the crucible technique. The fiber was then rapidly drawn from the outflow of the nozzles at the bottom of the silica crucible. No trace of crystallization was observed to the naked eye neither on the fiber, nor on the preform neck-down. About ten meters of crystal-free fibers were successfully and reproducibly produced from the 11 cm length preforms. Careful adjustments of the drawing process permit to control the core-cladding diameter ratio of the produced fibers. All the fibers produced were coated during the process with low index UV-cured polymer. A fiber cross-section image of the step-index fiber obtained by this modified crucible technique is shown in Fig. 7. The outer (cladding) and inner (core) diameters are 127 μm and 68 μm, respectively. Single-index fibers of same diameter made of 10BaPF90 glass were also produced by the same technique (not shown here).

The reason why this alternative technique has permitted to eliminate the surface crystallization during the fiber drawing still remains unclear and is currently under investigation. We believe that the risk of crystallization was strongly reduced by the combination of a higher temperature than that used in the preform drawing technique and the absence of contact of the outer preform surface with surrounding argon atmosphere. Nonetheless, this technique paves the way for drawing optical fibers from various exotic glasses that were initially discarded because of their strong tendency to crystallize during their drawing (e.g. fluorides, fluoroaluminates, etc.). The compatibility of the preform glass with the fused silica of the crucible at relatively high temperature (glass viscoelastic regime) also has to be considered. Surprisingly, no reaction between the fluorophosphate glass and the silica crucible was evidenced. Although the reusing of the silica crucible is difficult because removing all the residual fluorophosphate glass after drawing is not possible, unless by heating it at melting temperature, which results in strong interaction with the crucible walls.

As above mentioned, about 10 m of crystal-free step-index fiber

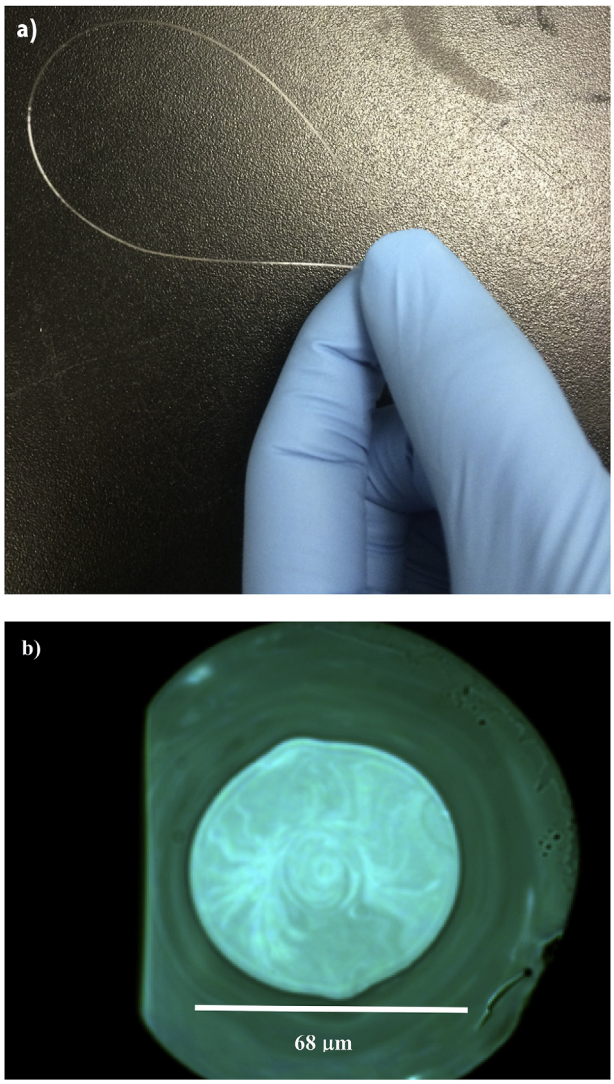

Fig. 7. Photograph of the fabricated optical fiber (a). Optical microscopy image of the optical step-index fiber section (127 μm diameter) without polymer coating (b).

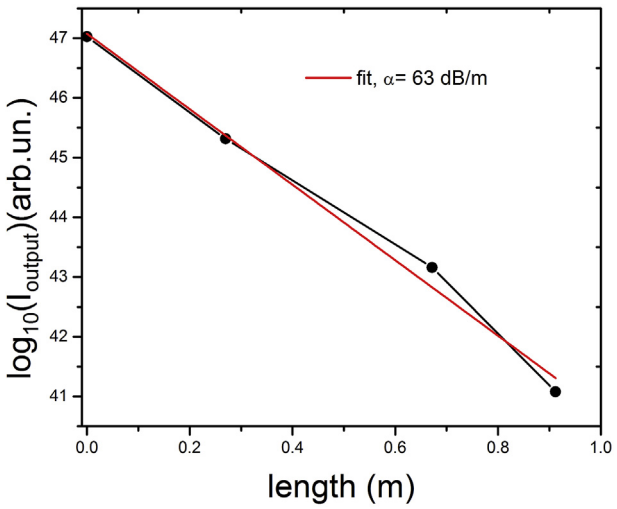

Fig. 8. Measured power output at 244 nm wavelength, recorded from a fiber initial section of 0.2 m. In red: best fit of the attenuation curve, weighted to the linear intensity of the signal. (For interpretation of the references to colour in this figure legend, the reader is referred to the web version of this article.)

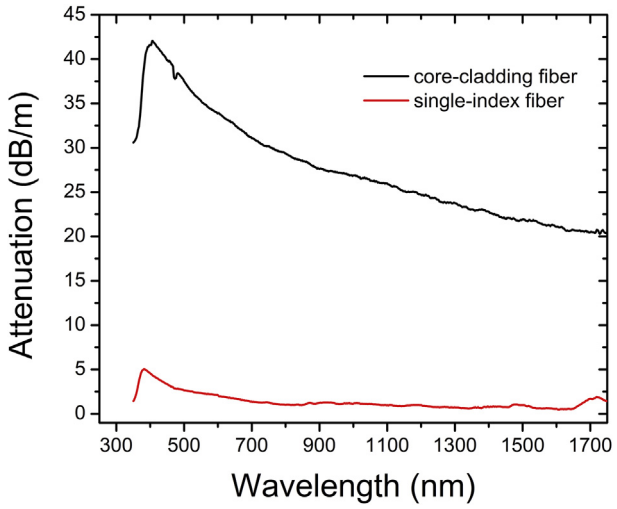

Fig. 9. Attenuation spectra of the single-index fiber (red curve) and core-cladding fiber (black curve) measured by the cut-back method on 3 fiber sections. (For interpretation of the references to colour in this figure legend, the reader is referred to the web version of this article.)

with homogeneous diameter can be fabricated with reproducibility from one single preform. For the optical losses characterization carried out by the cut-back technique, two different sections of optical fibers were used: the first one was initially of 6.5 m for the measurements in the 350 nm $\leq \lambda_2 \leq$ 1750 nm range and the second one of 0.2 m for the measurement at $\lambda_1 = 244$ nm. Such short piece of fiber had to be used to enable the detection of the output power in the DUV. As presented in Fig. 8, the optical losses at 244 nm were calculated to be 63 dB/m from the output intensity measured as a function of fiber length.

The optical attenuation spectrum recorded from the step-index fiber in the range 350 nm $\leq \lambda_2 \leq$ 1750 nm is presented in Fig. 9. For comparison, the same measurements were carried out on the single-index fibers fabricated. In the latter case, the low index polymer was intended to play the role of the optical cladding to enable light guiding by total internal reflection within the FP fiber. The losses decrease monotonously from 42 to 20 dB/m in the range 407–1750 nm. At 350 nm, an abrupt increase in the losses are observed possible because of metal impurities. For the single-index fiber, a similar behavior was observed but the total losses are approximately lower by an order of magnitude, from 5 dB/m to a minimum of ~0.7 dB/m. The high losses measured on the core-cladding fiber compared to the single-index fiber are probably due to extrinsic losses caused by imperfections in the core glass/clad glass interface. Optical microscope inspection of the fiber has revealed the presence of bubbles. Moreover, glass striae can be clearly observed (Fig. 7) in the core of the fiber, causing background absorption of light and increasing thus the losses. Work is ongoing to improve the fabrication process and eliminate these striae.

In the literature, as above mentioned, only four works dealing with the fabrication and optical characterization of fluorophosphate glass fibers was reported, to the best of our knowledge [17,18,22,23]. In their work, Zou et al. from Hoya Corporation reported ultra-low losses in their fibers with a minimum loss in the UV of 0.11 dB/m at 365 nm while extrinsic absorption bands were observed due to the presence of transition metal impurities at 340 nm (Fe^{3+}), 520 nm (Cr^{3+}, Ni^{2+}) and 800 nm (Cu^{2+}, Fe^{2+}) [17,18]. Second, Kalnins et al. reported in 2011 and 2016 minimum loss

values in the violet at 405 nm of 3.05 dB/m and 0.5–1.0 dB/m, respectively, from single-index fibers drawn from commercial fluoride-phosphate glasses (Schott N-FK51A). They systematically observed crystallization in the neck-down of the preform in each fiber drawing trial, like in our first experiments of drawing from the glass preforms. Their best results were achieved after improving the drawing process parameters [20] (e.g. by increasing the preform feed rate and drawing speed) and the preform surface quality [21]. In our work, the transmission losses measured on the single-index fiber, shown in Fig. 9, are in the same range (i.e. between 1 and 5 dB/m).

Therefore, the optical quality of the core-cladding fluorophosphate glass fibers have to be improved for the targeted applications in the VUV and DUV regions (e.g. fast remote elemental analysis of non-metallic elements as phosphorus). On one hand, the fabrication process through the modified crucible technique is still under development. On the other hand, important efforts are requested to remove specific impurities in the glass precursors: their concentration of transition metal ions like iron, nickel, copper and cobalt have to be reduced to below 10 ppb. A higher transmission in the UV region would be then expected in these fluorophosphate glass fibers, making them suitable candidates for optical materials capable to operate in the VUV and DUV regions. In parallel, numerical simulations considering the specific optical features of the fluorophosphate glasses are also ongoing to propose a simple design of microstructured hollow core fiber exhibiting an enhanced UV-light transmission.

4. Conclusion

Highly-pure fluorophosphate glasses with 10 mol % of barium polyphosphate and 90 mol% of fluorides have been prepared and showed to be suitable for fiber drawing thanks to their excellent thermal stability against crystallization of 149 °C. The studied bulk glasses also present optical transparency extending in the deep-UV region down to 180 nm, exhibiting a small absorption peak in this region due to the presence of Fe^{2+} traces impurity. Core-cladding preforms were produced by a modified built-in casting method. Step-index and Single-index optical fibers were then successfully fabricated from the as-prepared preforms through a fused silica crucible assembly. This alternative approach has permitted to get rid of the surface crystallization issues occurring during the drawing process and may pave the way to further fiber fabrication from glasses with strong tendency to surface crystallization. An optical attenuation of 63 dB/m and 20–42 dB/m was measured on the produced step-index fibers at 244 nm and in the range 407–1750 nm, respectively. For the single-index fiber, the optical losses in the range 407–1750 nm are 0.7–5 dB/m.

Despite the requested improvements in terms of glass chemical purity or fiber optical quality to envisage future optical applications using these fibers, the alternative fiber fabrication approach proposed in this work constitutes one avenue to address the challenges inherent to the complex fabrication of fluorophosphate glass fibers for photonics.

Acknowledgments

This research was supported by the Canadian Excellence Research Chair program (CERC) in Photonic Innovations. The authors are also grateful to the Natural Sciences and Engineering Research Council of Canada (NSERC), the Fonds de Recherche Québecois sur la Nature et les Technologies (FRQNT) (RS-144616), the Canadian Foundation for Innovation (CFI) (29191 and 32532) and the Brazilian agency Capes for the financial support.

References

[1] B. Welz, M. Sperling, Physical principles, in: At. Absorpt. Spectrom, Wiley-VCH Verlag GmbH, 1998, pp. 63–102.
[2] R.S. Harmon, R.E. Russo, R.R. Hark, Applications of laser-induced breakdown spectroscopy for geochemical and environmental analysis: a comprehensive review, Spectrochim. Acta Part B At. Spectrosc. 87 (2013) 11–26.
[3] R.E. Neuhauser, U. Panne, R. Niessner, Utilization of fiber optics for remote sensing by laser-induced plasma spectroscopy (LIPS), Appl. Spectrosc. 54 (2000) 923–927.
[4] S. Palanco, C. López-Moreno, J.J. Laserna, Design, construction and assessment of a field-deployable laser-induced breakdown spectrometer for remote elemental sensing, Spectrochim. Acta Part B At. Spectrosc. 61 (2006) 88–95.
[5] R. Noll, H. Bette, A. Brysch, M. Kraushaar, I. Mönch, L. Peter, V. Sturm, Laser-induced breakdown spectrometry — applications for production control and quality assurance in the steel industry, Spectrochim. Acta Part B At. Spectrosc. 56 (2001) 637–649.
[6] M. Oto, S. Kikugawa, N. Sarukura, M. Hirano, H. Hosono, Optical fiber for deep ultraviolet light 13 (2001) 978–980.
[7] A.N. Gurzhiev, L.K. Turchanovich, V.G. Vasilchenko, V.A. Bogatyrjov, V.M. Mashinsky, Radiation damage in optical fibers, Nucl. Instrum. Methods Phys. Res. Sect. Accel. Spectrom. Detect. Assoc. Equip. 391 (1997) 417–422.
[8] K.-F. Klein, C.P. Gonschior, D. Beer, H.-S. Eckhardt, M. Belz, J. Shannon, V. Khalilov, M. Klein, C. Jakob, Silica-based UV-fibers for DUV applications: current status, in: Proc. SPIE, 2013, p. 87750B.
[9] R.T. Williams, Vacuum ultraviolet properties of beryllium fluoride glass, J. Appl. Phys. 52 (1981) 6279.
[10] N. Kitamura, J. Hayakawa, H. Yamashita, Optical properties of fluoroaluminate glasses in the UV region, J. Non. Cryst. Solids 126 (1990) 155–160.
[11] H. Hefang, L. Fengying, Y. Yibo, F. Jitian, Crystallization of fluoroaluminate glasses, J. Non. Cryst. Solids 112 (1989) 306–308.
[12] U. Bärenwald, M. Dubiel, W. Matz, D. Ehrt, Structural models of the fluoroaluminate glass system $Ba(PO_3)_2$-CaF_2-AlF_3, J. Non. Cryst. Solids 130 (1991) 171–181.
[13] D. Ehrt, M. Leister, A. Matthai, Polyvalent elements iron, tin and titanium in silicate, phosphate and fluoride glasses and melts, Phys. Chem. Glas. 42 (2001) 231–239.
[14] D. Ehrt, REVIEW: phosphate and fluoride phosphate optical glasses — properties, structure and applications, Phys. Chem. Glas. Eur. J. Glas. Sci. Technol. Part B 56 (2015) 217–234.
[15] D. Ehrt, P. Ebeling, U. Natura, UV transmission and radiation-induced defects in phosphate and fluoride-phosphate glasses, J. Non. Cryst. Solids 263 (2000) 240–250.
[16] D. Möncke, D. Ehrt, L.L. Velli, C.P.E. Varsamis, E.I. Kamitsos, Structure and properties of mixed phosphate and fluoride glasses, Phys. Chem. Glas. J. Glas. Sci. Technol. Part B 46 (2005) 67–71.
[17] X. Zou, K. Itoh, H. Toratani, Transmission loss characteristics of fluorophosphate optical fibers in the ultraviolet to visible wavelength region, J. Non. Cryst. Solids 215 (1997) 11–20.
[18] X. Zou, H. Toratani, Radiation resistance of fluorophosphate glasses for high performance optical fiber in the ultraviolet region, J. Appl. Phys. 81 (1997) 3354–3362.
[19] D. Feng, Q. He, M. Lu, W. Li, W. Song, P. Wang, B. Peng, Investigations on the photoluminescence spectra and its defect-related nature for the ultraviolet transmitting fluoride-containing phosphate-based glasses, J. Non. Cryst. Solids 425 (2015) 130–137.
[20] U. Natura, T. Feurer, D. Ehrt, Kinetics of UV laser radiation defects in high performance glasses, Nucl. Instrum. Methods Phys. Res. Sect. B-Beam Interact. Mater. Atoms 166 (2000) 470–475.
[21] P. Wang, M. Lu, F. Gao, H. Guo, Y. Xu, C. Hou, Z. Zhou, B. Peng, Luminescence in the fluoride-containing phosphate-based glasses: a possible origin of their high resistance to nanosecond pulse laser-induced damage, Sci. Rep. 5 (2015) 8593.
[22] C.A.G. Kalnins, H.E. Heidepriem, A. Dowler, T.M. Monro, Fabrication of fluoride phosphate glass optical fibres for UV applications, in: Proc. Int. Quantum Electron. Conf. Conf. Lasers Electro-optics Pacific Rim 2011, Optical Society of America, Sydney (, 2011, pp. 2051–2053.
[23] C.A.G. Kalnins, N.A. Spooner, T.M. Monro, H. Ebendorff-Heidepriem, E. Bailey, Surface analysis and treatment of extruded fluoride phosphate glass preforms for optical fiber fabrication, J. Am. Ceram. Soc. 99 (2016) 1874–1877.
[24] M. Boivin, M. El-Amraoui, Y. Ledemi, S. Morency, R. Vallée, Y. Messaddeq, Germanate-tellurite composite fibers with a high-contrast step-index design for nonlinear applications, Opt. Mater. Express 4 (2014) 1740–1746.
[25] D. Manzani, Y. Ledemi, I. Skripachev, Y. Messaddeq, S.J.L. Ribeiro, R.E.P. De Oliveira, C.J.S. De Matos, Yb^{3+} Tm^{3+} and Ho^{3+} triply-doped tellurite core-cladding optical fiber for white light generation, Opt. Mater. Express 1 (2011) 1515–1526.
[26] G. Tao, H. Ebendorff-Heidepriem, A.M. Stolyarov, S. Danto, J.V. Badding, Y. Fink, J. Ballato, A.F. Abouraddy, Infrared fibers, Adv. Opt. Photonics 7 (2015) 379–458.
[27] H. Tokiwa, Y. Mimura, T. Nakai, O. Shinbori, Fabrication of long single-mode and multimode fluoride glass fibres by the double-crucible technique, Electron. Lett. 21 (1985) 1131–1132.
[28] P.A. Tick, N.F. Borrelli, I.M. Reaney, Relationship between structure and

transparency in glass-ceramic materials, Opt. Mater. Amst 15 (2000) 81–91.
[29] A. Galstyan, S.H. Messaddeq, V. Fortin, I. Skripachev, R. Vallée, T. Galstian, Y. Messaddeq, Tm^{3+} doped Ga–As–S chalcogenide glasses and fibers, Opt. Mater. Amst 47 (2015) 518–523.
[30] M.F. Churbanov, V.S. Shiryaev, A.A. Pushkin, V.V. Gerasimenko, A.I. Suchkov, V.S. Polyakov, V.V. Koltashev, V.G. Plotnichenko, Origin of micro-inhomogeneities in As-S-Se glass fibers fabricated by the double-crucible method, Inorg. Mater. 43 (2007) 436–440.
[31] J. Sanghera, I. Aggarwal, L. Busse, P. Pureza, V. Nguyen, R. Miklos, F. Kung, R. Mossadegh, Development of low loss IR transmitting chalcogenide glass fibers, in: Proc. SPIE 2396, Biomedical Optoelectronic Instrumentation, vol. 2396, 1995, pp. 71–77.
[32] J. Lapointe, Y. Ledemi, S. Loranger, V.L. Iezzi, E.S. de Lima Filho, F. Parent, S. Morency, Y. Messaddeq, R. Kashyap, Fabrication of ultrafast laser written low-loss waveguides in flexible As_2S_3 chalcogenide glass tape, Opt. Lett. 41 (2016) 203–206.
[33] T.S. Gonçalves, R.J. Moreira Silva, M. De Oliveira Junior, C.R. Ferrari, G.Y. Poirier, H. Eckert, A.S.S. De Camargo, Structure-property relations in new fluorophosphate glasses singly- and co-doped with Er^{3+} and Yb^{3+}, Mater. Chem. Phys. 157 (2015) 45–55.
[34] D. Ehrt, Fluoroaluminate glasses for lasers and amplifiers, Curr. Opin. Solid State Mater. Sci. 7 (2003) 135–141.
[35] B. Karmakar, P. Kundu, R.N. Dwivedi, UV transparency and structure of fluorophosphate glasses, Mater. Lett. 57 (2002) 953–958.
[36] D. Ehrt, W. Seeber, Glass for high performance optics and laser technology, J. Non. Cryst. Solids 129 (1991) 19–30.
[37] D. Ehrt, M. Carl, T. Kittel, M. Müller, W. Seeber, High-performance glass for the deep ultraviolet range, J. Non. Cryst. Solids 177 (1994) 405–419.
[38] R.K. Brow, Review: the structure of simple phosphate glasses, J. Non. Cryst. Solids 263 (2000) 1–28.
[39] H. Ebendorff-Heidepriem, T.M. Monro, Extrusion of complex preforms for microstructured optical fibers, Opt. Express 15 (2007) 15086–15092.
[40] D.C. Tran, G.H. Sigel, B. Bendow, Heavy metal fluoride glasses and fibers: a review, J. Light. Technol. 2 (1984) 566–586.
[41] T. Iqbal, M.R. Shahriari, P. Foy, G.H. Sigel, Preliminary study of fiber drawing of AlF_3-based glasses, Mater. Sci. Eng. B 12 (1992) 299–303.